Supplementary document of “Spatio-Spectral Correlations in Interferenceless Coded Aperture Correlation Holography with Vortex Speckles”

Eulàlia Puig Vilardell,[a,b,c,*] Shivasubramanian Gopinath,[a] Vipin Tiwari,[a] Tauno Kahro,[a] Aarne Kasikov,[a] Markus Kõiv,[a] Andra Naresh Kumar Reddy,[d] Joseph Rosen,[e] Kaupo Kukli,[a] Darius Gailevičius,[b] Saulius Juodkazis,[c,f] Vijayakumar Anand[a,c]

[a]Institute of Physics, University of Tartu, W. Ostwaldi 1, 50411 Tartu, Estonia
[b]Laser Research Center, Physics Faculty, Vilnius University, Sauletekio Ave. 10, 10223 Vilnius, Lithuania
[c]Optical Sciences Centre and ARC Training Centre in Surface Engineering for Advanced Materials (SEAM), School of Science, Computing and Engineering Technologies, Swinburne University of Technology, Hawthorn, VIC 3122, Australia
[d]Laboratory of Nonlinear Optics, Institute of Astronomy, University of Latvia, Jelgavas 3, LV-1004 Riga, Latvia
[e]School of Electrical and Computer Engineering, Ben Gurion University of the Negev, P.O. Box 653, Beer-Sheva 8410501, Israel
[f]Tokyo Tech World Research Hub Initiative (WRHI), School of Materials and Chemical Technology, Tokyo Institute of Technology, 2-12-1, Ookayama, Meguro-ku, Tokyo 152-8550, Japan

1. Depth Wavelength Reciprocity in Refractive and Diffractive Optics

Most of the CAI and I-COACH methods use coded masks that are predominantly diffractive in nature. The research problem is shown in Fig. S1 by comparing a simple single element imaging system using a refractive (Fig. S1(a)) and a diffractive lens (Fig. S1(b)) for imaging a point. A diverging spherical wavefront from a point object is converted into a converging spherical wavefront using the lens. Using Fresnel approximation, the phase error function can be expressed as $\Phi_e = \left\{\frac{exp\left(j\frac{\pi}{\lambda_p u_q}R^2\right)exp\left(-j\frac{\pi}{\lambda f}R^2\right)exp\left(j\frac{\pi}{\lambda_p v}R^2\right)}{\left[exp\left(j\frac{\pi}{\lambda u}R^2\right)exp\left(-j\frac{\pi}{\lambda f}R^2\right)exp\left(j\frac{\pi}{\lambda v}R^2\right)\right]}\right\}$, where p and q are integers varying from 1 to m. Considering a typical case, $u = v = 2f$ with a magnification $M = 1$, the above error function is solved for changes in depth from f to $u + f$ and wavelength over the visible region 400 nm to 600 nm with the design wavelength at the He-Ne red laser’s central wavelength 632.8 nm. The root mean square error (RMSE) of $arg(\Phi_e)$ for the refractive and diffractive cases are shown in Fig. S1(c) and Fig. S1(d) respectively. The variation of the normalized intensity value at the origin of the intensity distribution at the image sensor for the changes in depth and wavelength for the refractive and diffractive cases are shown in Fig. S1(e) and Fig.

S1(f) respectively. It must be noted that the reference imaging system can have a refractive lens or a harmonic lens[1] or a multi-order diffractive lens[2] or a wavelength insensitive engineered diffractive element.[3] From Figure S1, the problem that is addressed in this study is presented clearly. With a diffractive lens, a certain phase distribution at the lens and certain intensity distribution (sharp focus point) at the image sensor can be obtained for different conditions of depth and wavelength. However, for a refractive imaging system, neglecting mild dispersion effects, there is only one condition of depth, where a certain phase distribution at the lens and certain intensity distribution at the image sensor can be obtained. The consequence of DWR in I-COACH for sensing applications is significant increasing uncertainties in the measurement.

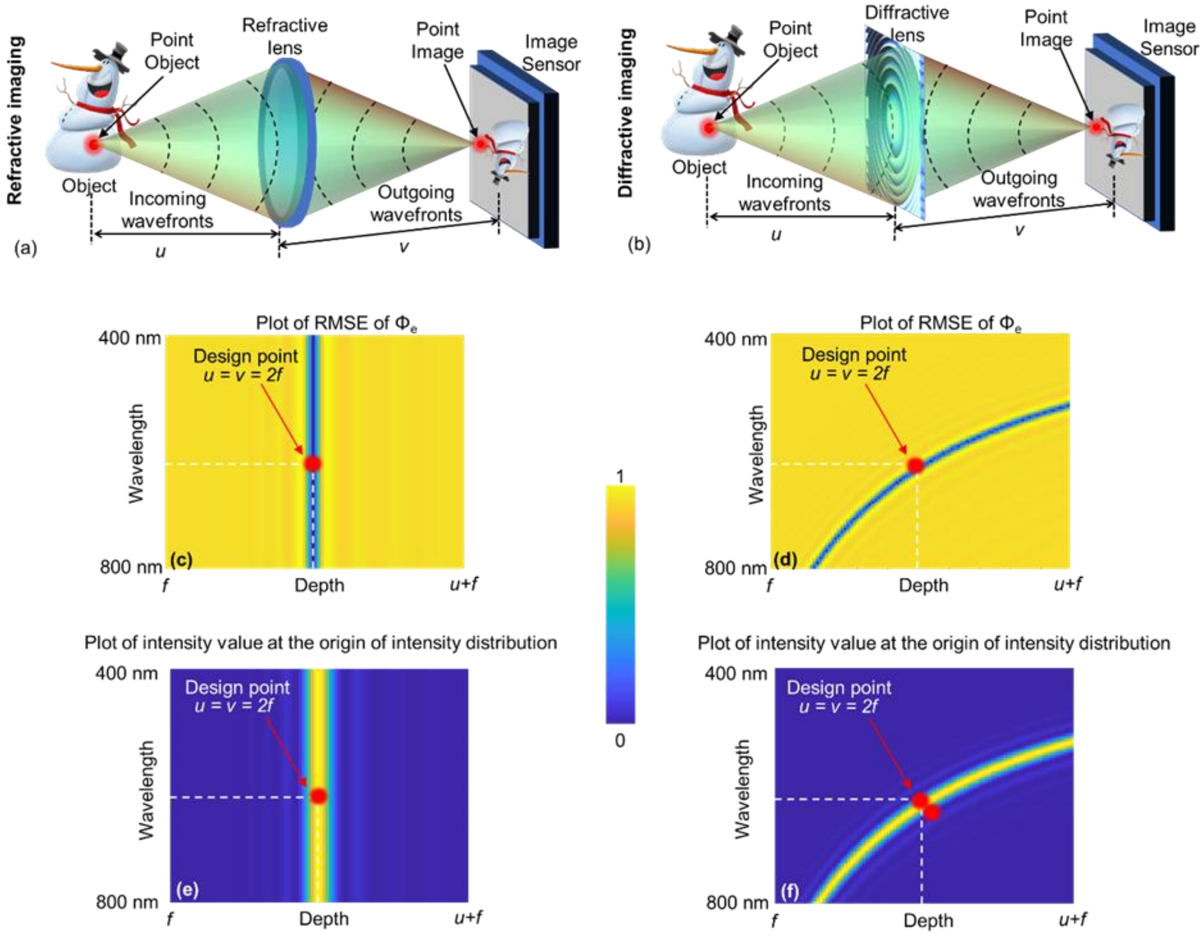

Fig. S1 Optical configuration of (a) refractive imaging and (b) diffractive imaging. Plot of RMSE of $arg(\Phi_e)$ for (c) refractive imaging and (d) diffractive imaging. Plot of intensity value at the origin of the intensity distribution on the image sensor for (e) refractive imaging and (f) diffractive imaging.

2. Fabricated devices

An extended version of the Polarized Optical Microscopy (OM) and Scanning Electron Microscope images (SEM) including all the fabricated devices is presented in Fig. S2.

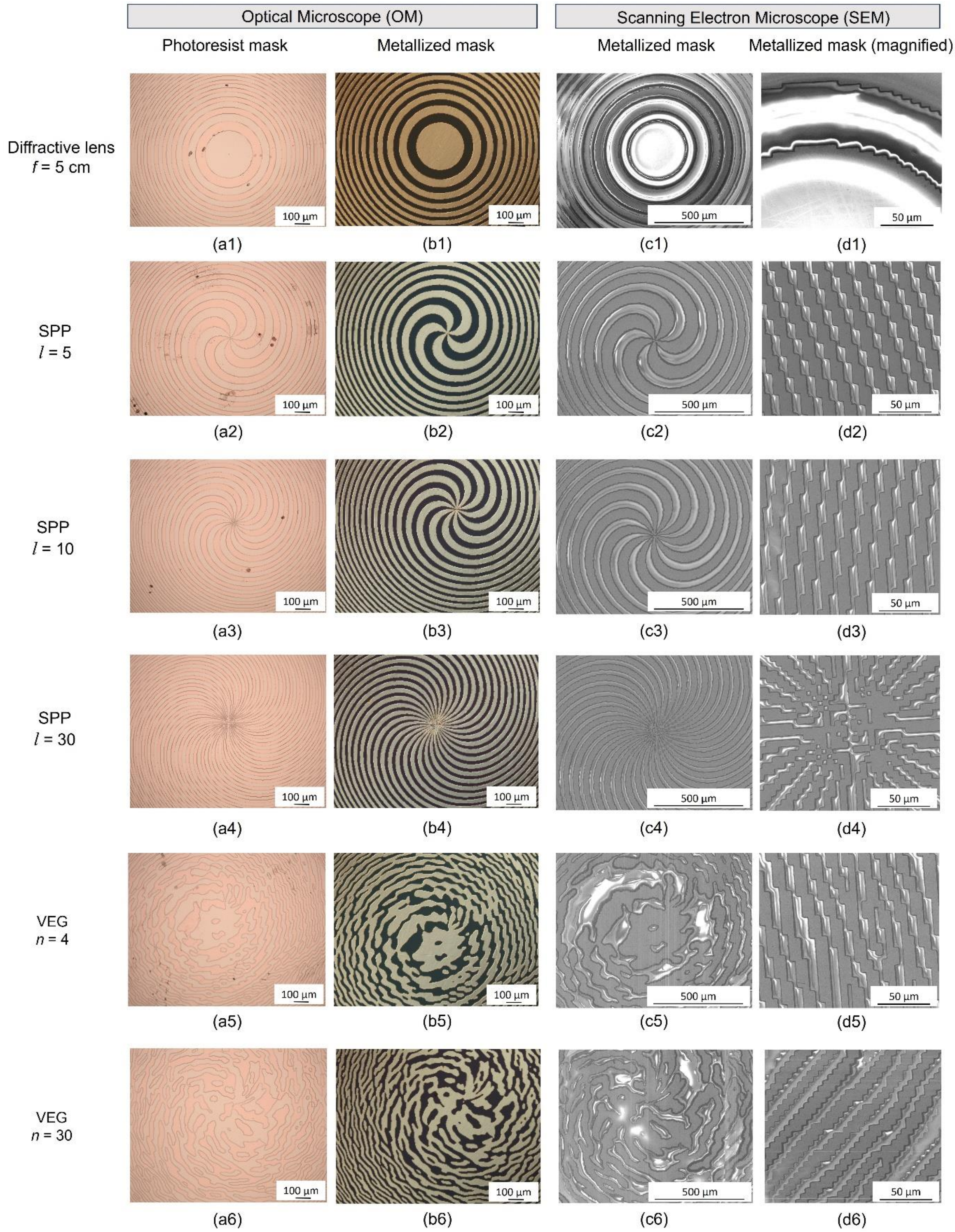

Fig. S2 Polarized Optical Microscopy images (OM) and Scanning Electron Microscope images (SEM) of all the fabricated devices. (a1 – d1) Diffractive lens f = 5 cm, (a2 – d2) SPP l = 5, (a3 – d3) SPP l = 10, (a4 – d4) SPP l = 30, (a5 – d5) VEG n = 4, (a6 – d6) VEG n = 30.

3. Lucy-Richardson Rosen Algorithm (LRRA)

The Lucy-Richardson-Rosen algorithm (LRRA) is a well-established deconvolution algorithm which has been developed by combining two deconvolution algorithms, i.e., non-linear reconstruction (NLR) [4] and Lucy-Richardson algorithm (LRA) [5,6]. In NLR, the reconstructed image is optimized by tuning two non-linear parameters, i.e., α and β between -1 and 1 to obtain minimum entropy. On the other hand, LRA uses an iterative approach, where the reconstructed image is iterated in a loop until an optimal reconstruction is achieved. The LRA consists of a forward convolution between the approximate solution and the I_{PSF} and a backward correlation between the I_{PSF} and the ratio between I_O and the estimated solution. This ratio is multiplied by the previous solution, and this process is continued until an optimal solution is obtained. In LRRA, the backward correlation (matched filter) is replaced by NLR. LRRA leverages the combined approach of NLR and LRA, yielding a better estimation of reconstructed images with a rapid convergence [7].

In LRRA, the reconstructed image is given as

$$I_R(p) = I_R(p-1)\left[\frac{I_O}{I_R(p-1)\otimes I_{PSF}} *_{\beta}^{\alpha} I_{PSF}\right] \tag{S1}$$

where '$*_{\beta}^{\alpha}$' is the non-linear reconstruction operator given as $u *_{\beta}^{\alpha} v = \mathcal{F}^{-1}\{|U|^{\alpha}|V|^{\beta}\exp(i\Phi_U)\cdot\exp(-i\Phi_V)\}$, where U and V are the Fourier transforms of u and v respectively. p is the number of iterations. The schematic (flowchart) of LRRA is shown in the Figure S3.

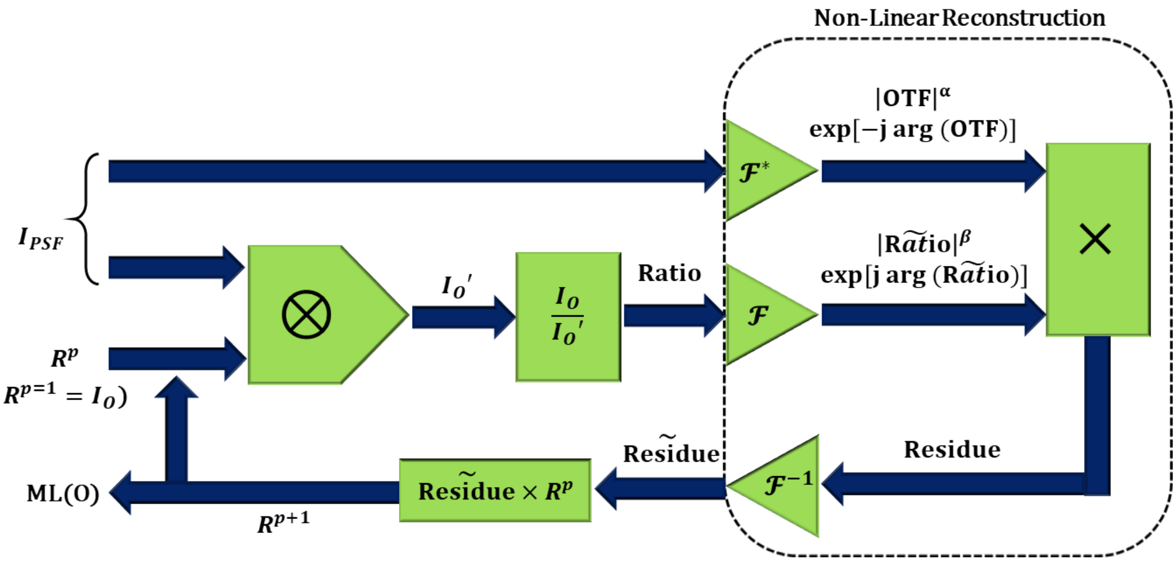

Figure S3. Schematic of the Lucy–Richardson–Rosen algorithm. OTF – optical transfer function; *p*—number of iterations of LRRA; ⊗—2D convolutional operator; R^p is the p^{th} solution; and *p* is an integer; when $p = 1$, $R^p = I_O$; and α and β are varied from -1 to 1; ~ Fourier transform; '*' complex conjugate; NLR is a nonlinear reconstruction; and $\mathcal{F}$ and $\mathcal{F}^{-1}$ are Fourier and inverse Fourier transforms, respectively.

References

1. D. W. Sweeney and G. E. Sommargren, Harmonic diffractive lenses. *Appl. Opt*. 34(14), 2469-2475 (1995).

2. D. Faklis and G. M. Morris, Spectral properties of multiorder diffractive lenses. *Appl. Opt*. 34(14), 2462-2468 (1995).

3. N. Mohammad, M. Meem, B. Shen, P. Wang, and R. Menon, Broadband imaging with one planar diffractive lens. *Sci. Rep*. 8(1), 2799 (2018).

4. M. R. Rai, V. Anand, J. Rosen, Non-linear adaptive three-dimensional imaging with interferenceless coded aperture correlation holography (I-COACH). *Opt Express* 26, 18143–18154 (2018).

5. W. H. Richardson, Bayesian-based iterative method of image restoration, *J. Opt. Soc. Am*, 62, 55-59 (1972).

6. L. B. Lucy, An iterative technique for the rectification of observed distributions, *Astron J*, 79, 745 (1974).

7. V. Anand, M. Han, J. Maksimovic, S. H. Ng, T. Katkus, A. Klein, K. Bambery, M. J. Tobin, J. Vongsvivut, and S. Juodkazis, "Single-shot mid-infrared incoherent holography using Lucy-Richardson-Rosen algorithm," *Opto-Electron. Sci*. 1, 210006 (2022).